Chinese Chemical Letters 36 (2025) 110439

Contents lists available at ScienceDirect

Chinese Chemical Letters

journal homepage: www.elsevier.com/locate/cclet

Elucidating oxygen evolution and reduction mechanisms in nitrogen-doped carbon-based photocatalysts

Yan Wang[a], Jiaqi Zhang[a], Xiaofeng Wu[b,c], Sibo Wang[a], Masakazu Anpo[a], Yuanxing Fang[a,b,*]

[a] State Key Laboratory of Photocatalysis on Energy and Environment, College of Chemistry, Fuzhou University, Fuzhou 350116, China
[b] Sino-UK International Joint Laboratory on Photocatalysis for Clean Energy and Advanced Chemicals & Materials, Fuzhou University, Fuzhou 350108, China
[c] Department of Chemistry and Materials Innovation Factory, University of Liverpool, Liverpool L69 7ZD, United Kingdom

ARTICLE INFO

Article history:
Received 12 May 2024
Revised 6 September 2024
Accepted 9 September 2024
Available online 10 September 2024

Keywords:
Nitrogen-doped carbon
Chemical vapor deposition
Photocatalysis
Water oxidation reaction
Oxygen reduction reaction

ABSTRACT

Solar-induced water oxidation reaction (WOR) for oxygen evolution is a critical step in the transformation of Earth's atmosphere from a reducing to an oxidation one during its primordial stages. WOR is also associated with important reduction reactions, such as oxygen reduction reaction (ORR), which leads to the production of hydrogen peroxide (H_2O_2). These transitions are instrumental in the emergence and evolution of life. In this study, transition metals were loaded onto nitrogen-doped carbon (NDC) prepared under the primitive Earth's atmospheric conditions. These metal-loaded NDC samples were found to catalyze both WOR and ORR under light illumination. The chemical pathways initiated by the pristine and metal-loaded NDC were investigated. This study provides valuable insights into potential mechanisms relevant to the early evolution of our planet.

The transition of a reducing atmosphere, mainly comprising NH_3 and CH_4 in Earth's primordial state to an oxidizing one, consisting of O_2 and N_2, played a pivotal role in the emergence of life. The solar-induced water oxidation reaction (WOR) for oxygen evolution has been suspected to play a critical role in achieving this transformation [1–4]. Evidence has revealed that both anoxygenic and oxygenic photosynthesis were capable of releasing O_2 gas from water, with traces of such processes dating back to the Archean Eon, as early as 2.5 billion years ago [5,6]. Moreover, WOR is also significant as it is associated with a series of important reduction reactions [7–12]. For instance, H_2O_2 production can be achieved by an oxygen reduction reaction (ORR), another spontaneously crucial reaction for life evolution [13,14]. In plant cells, the peroxidase enzyme leads to an efficient transfer of electrons to O_2 molecules under sunlight irradiation, resulting in the generation of superoxide. Subsequently, the action of dismutase on the superoxide leads to the formation of H_2O_2 [15], and it can be further utilized by organisms to combat pathogens [16]. The importance of both these reactions has stimulated us to investigate the origins of photoactive mediators beyond the realm of photosynthesis

Aiming to simulate the conditions of the Archean Eon, nitrogen-doped carbon (NDC) materials prepared by plasma-enhanced chemical vapor deposition (PE-CVD) was conducted. This process employed CH_4 and NH_3 gases as precursors and was carried out at a relatively low temperature of ~170 °C [17]. Notably, these NDC materials have demonstrated activities in photocatalytic redox reactions without the need for any additional co-catalysts. Furthermore, the carbon and nitrogen sites within the NDC have been identified to be responsible for driving reduction and oxidation reactions, respectively.

On another hand, the occurrence of an impact event has been proposed as a mechanism for the formation of metals on the early Earth [18–20]. Subsequently, compelling evidence indicates the widespread availability of various metal ions in the Archean Ocean, including Fe, Co, Ni, Cr, Zn, Cu, Mn, Pd, Ag and others [21–27]. Metals and carbon-based materials are known to have been present in the primordial stages of Earth, and metal- and nitrogen-rich carbon materials have also been found in meteorites [28–32]. This fact inspires us to consider the possibility of incorporating these metal ions with NDC materials to drive WOR and ORR using solar energy. Noted that in the field of photocatalysis, studies have been widely conducted by incorporation of metal/metal oxides on carbon materials for water redox reactions [33–35].

The water oxidation reaction (WOR) and ORR are reverse reactions, and their general processes are depicted in Scheme 1. In the WOR cycle, H_2O undergoes a two-electron process to form H_2O_2, while a four-electron process converts H_2O into O_2. Conversely, in

* Corresponding author.
E-mail address: yxfang@fzu.edu.cn (Y. Fang).

https://doi.org/10.1016/j.cclet.2024.110439
1001-8417/

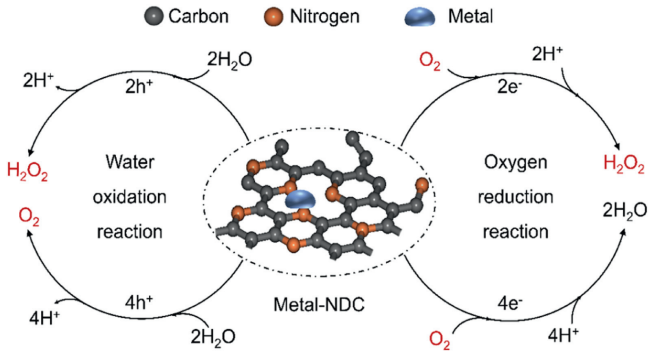

Scheme 1. Schematic illustration of WOR and ORR of metal-loaded NDC photocatalysts.

the ORR, O_2 can be transformed into H_2O_2 or H_2O through two- or four-electron processes, respectively [36–42]. These pathways typically involve the rearrangement of O—H and O—O bonds with the involvement of various intermediates, including *OH, *O, *OOH, *OO, and others [43–48]. However, the specific pathway can vary for each reaction, mainly depending on the active site in the photocatalytic system. Therefore, there is a strong motivation to uncover the operational mechanisms of these reactions using this unique NDC photocatalyst.

Herein, various metals were loaded on NDC to presumably mimic materials in the primitive Earth. These materials were then employed as photocatalysts to drive both WOR and ORR under light illumination. Specifically, the pristine NDC photocatalyst exhibited oxygen evolution reaction (OER) activity in the presence of electron scavengers, and when metal was loaded with NDC, the OER rate was notably improved. The metal-loaded NDC was also capable of driving ORR, which occurred OER simultaneously, resulting in an overall solar-to-chemical conversion. The chemical pathways of the OER and ORR on NDC-based photocatalysts were explored, highlighting the significance of carbon and nitrogen sites in activating O_2 and H_2O molecules, respectively. Moreover, the key role of metal on NDC was unveiled. Concerning OER, the presence of metal on NDC associated with the acceleration of the rate-determining step (RDS), namely the conversion from *—OH to *—OOH, thereby improving the OER performance. Only when metal was loaded on NDC, the ORR was witnessed for H_2O_2 production since metal species facilitated the conversion from O_2 to *OOH, a sluggish step in H_2O_2 production. These findings provide deep insight into the potential mechanisms relevant to the early evolution of Earth and contribute to the understanding of the chemical processes that shaped our planet.

The pristine NDC materials were synthesized based on our previous work, and the optimal NDC was applied for the subsequent studies [17]. The resultant materials were characterized by X-ray diffraction (XRD, Fig. S1 in Supporting information), scanning electron microscope (SEM, Fig. S2 in Supporting information), scanning transmission electron microscopy (STEM, Fig. S3 in Supporting information), X-ray photoelectron spectroscope (XPS, Fig. S4 in Supporting information), Fourier transform infrared (FTIR, Fig. S5 in Supporting information), solid-state ^{13}C nuclear magnetic resonance (^{13}C NMR, Fig. S6 in Supporting information), ultraviolet-visible diffuse reflectance spectroscopy (UV–vis DRS) (Fig. S7 in Supporting information), Raman spectroscopy (Fig. S8 in Supporting information). The analyses and discussions of the results can be found in Supporting information, and all the results from pristine NDC materials are undoubtedly consistent with the previous work.

Metals, including Co, Ni, Mn, Fe, Pd, Cr, Zn and Cu, were physically loaded on NDC. The loaded metals were investigated by inductively coupled plasma optical emission spectrometer, and the results were analyzed in Table S1 (Supporting information). All the loaded metals on NDC were detected, and their weight percentage was ~0.5%. The Co, Mn, and Zn loaded NDC were namely Co-NDC, Mn-NDC and Zn-NDC, respectively, and they were selected as typical examples for further investigation using XPS, as shown in Figs. 1a-c. There were four peaks observed in the spectrum of the Co 2p orbital (Fig. 1a). Among them, two peaks at 803.3 and 796.6 eV were attributed to the Co $2p_{1/2}$ satellite and Co $2p_{1/2}$ orbitals, respectively. The other pair at 786.2 and 780.6 eV were assigned to Co $2p_{3/2}$ satellite and Co $2p_{3/2}$ orbitals, respectively. Therefore, Co can be identified as Co(II) species [49,50]. In the spectrum of the Zn 2p orbital (Fig. 1b), two distinct peaks were observed at 1044.4 and 1021.7 eV, which were defined as Zn $2p_{1/2}$ and Zn $2p_{3/2}$ orbital, respectively, confirming the presence of the Zn(II) species [51–54]. Four peaks were assigned from the spectrum of Mn 2p orbitals (Fig. 1c). Among them, two peaks at 653.5 and 651.9 eV were attributed to the Mn $2p_{1/2}$ satellite and Mn $2p_{1/2}$ orbitals, respectively. The other pair at 645.5 and 641.4 eV were assigned to Mn $2p_{3/2}$ satellite and Mn $2p_{3/2}$ orbitals, respec-

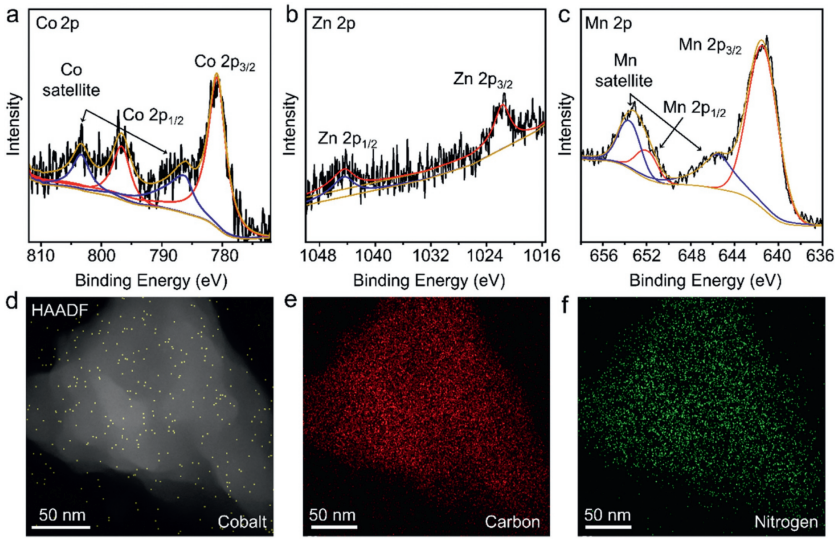

Fig. 1. High-resolution XPS spectra of (a) Co 2p, (b) Zn 2p, and (c) Mn 2p. HAADF images of Co-NDC along with EDX elemental maps showing (d) cobalt, (e) carbon, and (f) nitrogen.

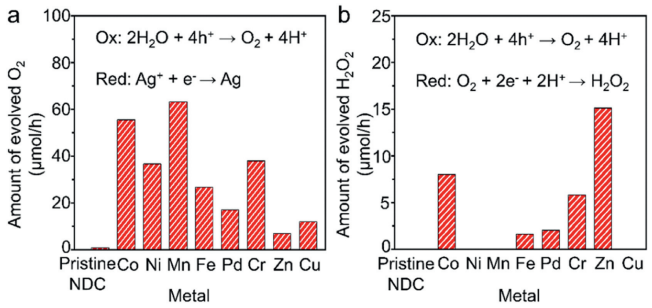

Fig. 2. (a) OER rate and (b) H_2O_2 production rate by ORR using NDC based photocatalysts with certain metal.

tively. Therefore, Mn can be identified as the mixture of Mn(II) and Mn(III) species, respectively [55–58]. In addition, the C 1s (Fig. S9a in Supporting information) and N 1s (Fig. S9b in Supporting information) spectra were acquired, and the C 1s peaks were presented as similar profile as that without loading any metals. While the N 1s peaks shifted to higher binding energy with respect to that of the pristine NDC. As such, the metal loadings highly affect the nitrogen species [59]. As a typical example, the Co-NDC was further investigated by transmission electron microscope (TEM). The TEM images, including high-angle annular dark-field (HAADF) images, are presented in Figs. S10a and b (Supporting information), respectively. These images suggest the formation of Co species on the NDC surface resembling a powdery structure. Upon analyzing Fig. S10a, the corresponding particle size analysis of the loaded Co species indicates an average size of approximately 8.46 nm (Fig. S10c in Supporting information). Moreover, high-resolution TEM images in Figs. S10d and e (Supporting information) have shown a lattice spacing of 0.213 nm, corresponding well to the (200) plane of cubic CoO [60], consistent with the Co 2p XPS results. Furthermore, energy dispersive X-ray spectrometry (EDX) mapping analysis, revealing the homogeneous distribution of Co, C, N, and O elements in Figs. 1d-f and Fig. S11 (Supporting information), respectively. This observation further confirmed the uniform anchoring of Co on NDC. In addition, the light absorption of the Co-NDC was investigated by UV–vis DRS, and the absorption spectrum is preserved as the pristine NDC (Fig. S12 in Supporting information), revealing, by such amount loading, metal has minor effect on the light absorption for NDC photocatalysts.

The photocatalytic OER and ORR were performed by 50 mg of photocatalysts. A 300 W Xenon lamp was applied as light source and Ag(I) was used as sacrifice agent for OER. The photocatalytic redox reactions and OER rates were shown in Fig. 2. Without any metal cocatalyst, the optimal NDC sample achieved the OER rate of ~0.8 μmol/h (Fig. S13 in Supporting information). Upon loading metals onto the NDC, the photocatalytic OER performances improved (Fig. 2a). Notably, the NDC photocatalyst loaded with Mn achieved the highest OER rate, with a value of 63.2 μmol/h, while the Co-NDC photocatalyst demonstrated a comparable result with an OER rate of 55.5 μmol/h. The optimal loading amount of Mn was determined to be 3 wt% (Fig. S14a in Supporting information).

NDC based photocatalyst was further applied for the H_2O_2 production by ORR, and OER was accompanied as oxidation reaction, resulting an overall solar-to-chemical conversion. The performances were presented in Fig. 2b. The pristine NDC is inactive, and Co, Fe, Pd, Cr, and Zn loaded NDC have presented photoactivities for H_2O_2 production. Among them, Zn-NDC presented the highest rate for H_2O_2 production at 15.1 μmol/h, and Co-NDC achieved a rate of 8.0 μmol/h. The optimal loading amount of Zn was determined to be 2 wt% (Fig. S14b in Supporting information). The reactions were further corroborated using $H_2{}^{18}O$ isotope, and the synthesis of $^{18}O_2$ during H_2O_2 production confirmed the overall redox nature of the reaction for solar-to-chemical conversion (Fig. S15 in Supporting information). Specifically, H_2O_2 and O_2 were produced by photoexcited electron and hole, respectively.

Notably, the optimal AQY for O_2 evolution is achieved ~19.8% and 33.69% at the wavelength of 420 nm and 365 nm, respectively. The performance exceeds that of graphitic carbon nitride (g-C_3N_4) and borocarbonitride (BCN) photocatalysts (Fig. S16 in Supporting information). The AQY for H_2O_2 evolution was found to be 0.09% and 0.23% at the corresponding wavelengths (Fig. S17 in Supporting information). The trend of AQY values generally aligns with the absorption spectrum of NDC, indicating that the redox reaction is driven by light illumination. In addition, by a four-cycle experiment (4 h per cycle), the performances were generally preserved (Fig. S18 in Supporting information). Characterizations, including FTIR and XPS, were conducted after the four-cycle photocatalytic reaction. Unobvious differences of spectra revealed that the photocatalysts were photochemically stable for the reactions (Figs. S19 and S20 in Supporting information).

To assess the enhanced performance, the reaction mechanism of NDC-based photocatalysts was further investigated. Since Co-NDC photocatalyst presented excellent performances for both OER by water splitting and ORR for H_2O_2 production, it was chosen as a typical example for in-depth investigation through steady-state and *in-situ* characterizations. Initial studies were conducted by steady-state characterizations. Time-resolved photoluminescence (TRPL) was applied to investigate the lives of the photoexcitation charges. The decay time of Co-NDC was measured at 1.89 ns, whereas it was 1.07 ns for pristine NDC (Fig. S21 in Supporting information). This result indicates that the presence of metal species on NDC contributes to an improvement in the lifetime of photoexcited charges, since the metal is likely to accumulate the charges [41,61,62].

In-situ FTIR was subsequently acquired to study the mechanisms for both OER and ORR. In the OER experiment, a reference experiment was first performed by pumping Ar gas into the system that containing Co-NDC. As the spectrum shown in Fig. 3a (curve 1), no significant peak was observed, indicating that the photocatalytic system remained inert in the presence of noble gas. When pure H_2O was introduced into the system, three distinct peaks were observed, including a broad absorption band and two weak peaks as shown in Fig. 3a (curve 2). Notably, a broad peak ranging from 3640 cm^{-1} to 3050 cm^{-1} was attributed to the stretching vibration of the O−H bond [63,64]. The weak peaks at 1645 cm^{-1} and 1536 cm^{-1} were assigned to the bending vibration of H−O−H in H_2O molecules and stretching vibration of N−O, respectively [65]. In addition, by increasing the quantity of the introduced water, the peaks at 2784, 2247, 2183 cm^{-1} and 1508 cm^{-1} gradually increased (Fig. S22a in Supporting information), and the peaks were assigned as O−H, N=C=O, C=C=O and N−O stretching vibration, respectively [66,67]. These signals indicated that H_2O molecules strongly interact with carbon and nitrogen site on NDC photocatalysts. By introducing Ag(I) solution into the system (Fig. S22b in Supporting information), a new absorption band locating at 1743 cm^{-1} gradually formed (Fig. 3a, curve 3), and this peak could be assigned to the C=O stretching vibration [68]. Meanwhile, the peaks at 3042–2800 cm^{-1} gradually decreased, and the peaks were assigned to the C−H stretching vibration (Fig. 3a, curve 3 and Fig. S22b). These observations suggested that the N=C−H/C=C−H dangling bonds reacted with H_2O to result N=C=O/C=C=O bonds.

When light illuminates the photocatalytic system that containing Co-NDC and Ag(I), inverted peaks emerge at 3640–3050 cm^{-1} and 1645 cm^{-1} formed as shown in Fig. 3a (curve 4). These peaks were owing to the O−H and H−O−H vibration modes of H_2O, respectively. This observation suggests that the H−O bonds of H_2O molecules on Co-NDC gradually dissociated. However, when Ag(I) was not added to the system and light illuminate it, the FTIR spectrum remains unchanged from the initial state (Fig. S23 in

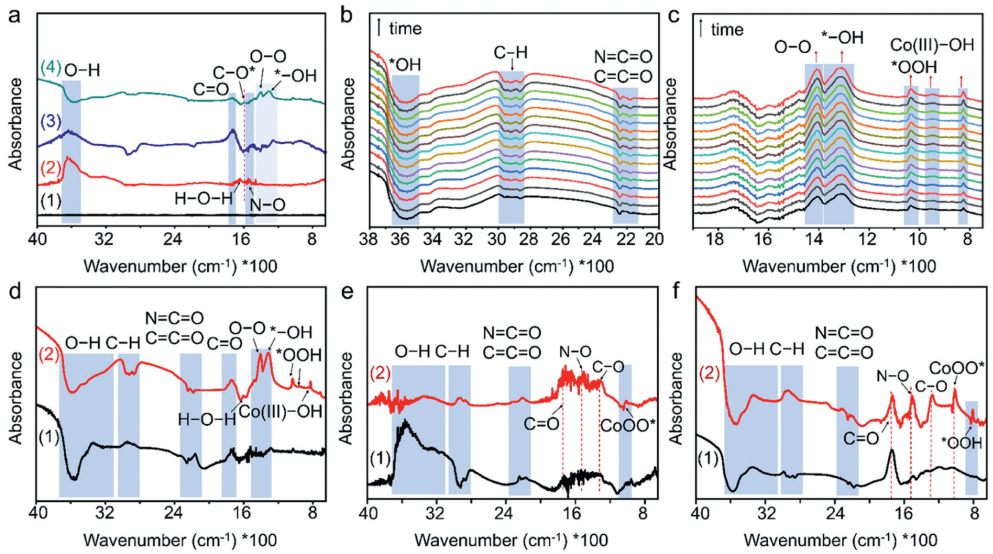

Fig. 3. (a) The FTIR spectra by pumping (1) Ar, (2) H_2O vapor, (3) Ag(I) solution, and (4) light illumination. (b, c) The time course of the FTIR spectra during the OER reaction. (d) The FTIR spectra of (1) NDC and (2) Co-NDC for OER under light illumination. (e) The FTIR spectra of (1) NDC, (2) Co-NDC by pumping O_2 gas without any light illumination and (f) the corresponding FTIR spectra with light illumination for ORR and OER.

Supporting information). This outcome indicates that without the presence of an electron scavenger like Ag(I), the OER reaction cannot be initiated.

Subsequently, time-resolved FTIR spectroscopy was performed to monitor the evolution of the OER under light illumination (Figs. 3b and c). Notably, the peak associated with the stretching vibration of C–H bonds (3042–2800 cm^{-1}) gradually decrease over time. Simultaneously, the other peaks corresponding to *–OH (1320 cm^{-1}), *–OOH (1037 and 948 cm^{-1}), and O–O (1408 cm^{-1}) gradually increase in intensity [69,70]. These identified species were known as the key intermediates during the OER of water splitting, revealing the dissociation of the H_2O and production of O_2 gas. Comparing the behavior of pristine NDC with Co-NDC under ambient conditions (Fig. S24 in Supporting information), no significant difference was observed. When both light illumination and Ag(I) were introduced into the system, the FTIR spectra of pristine NDC resembled those of Co-NDC (Fig. S25 in Supporting information), implying that the reaction pathways for OER were generally similar between the two.

Of particular importance was the observation of a distinct peak at 830 cm^{-1} in the Co-NDC spectrum, which could be attributed to the presence of Co(III)–OH species as shown in Fig. 3d [71]. This observation suggested that Co species also interacted with H_2O molecules, thereby facilitating the activation the *–OH. Consequently, this interaction significantly promoted the RDS in the OER, namely the conversion from *–OH to *–OOH.

The investigations of the ORR for H_2O_2 production by both pristine NDC and Co-NDC was further performed using *in-situ* FTIR. The background FTIR spectrum was collected with H_2O present in the system. When O_2 molecules were introduced into the systems, the resulting spectra are presented in Fig. 3e. For both Co-NDC and NDC photocatalysts, two peaks were observed at 1512 and 1280 cm^{-1}, and they were attributed to stretching vibrations of N–O and C–O bonds, respectively [72-74]. This result indicates that both nitrogen and carbon sites have the capability to adsorb O_2 molecules. More importantly, for Co-NDC sample, it is able to observe a distinct peak at 1014 cm^{-1}, which is owing to the CoOO* species [75]. This observation reveals that the Co sites is also capable of adsorbing O_2 molecules.

When light illuminates the photocatalytic system, notable difference was realized between Co-NDC and NDC (Fig. 3f). In the NDC spectrum, the intensities of both C–O and N–O peaks were generally sustained. In contrast, in Co-NDC, there is a significant enhancement in the peak intensities corresponding to C–O bond, N–O bond, and CoOO* species. This observation suggests Co is the key sites to initiate the activation of O_2 species. The photogenerated charges were possible injected from either Co or C species to the activated O_2 to form CoOO* species. It is noteworthy that in the absence of any metal on NDC, the active O_2 molecules on both carbon and nitrogen sites of pristine NDC cannot be converted to H_2O_2. Only when Co was loaded on NDC, photoexcited electrons could be injected into the Co species and O_2, which then could drive the transition from O_2 to OOH* species, the RDS in ORR for H_2O_2 production [76–78]. Simultaneously, in the spectrum of Co-NDC, the peaks for the conversion of H_2O molecules to O_2 molecules were observed, indicating OER was concurrently occurring.

On basis of the results from FTIR, Fig. 4 illustrates the pathways for both OER and ORR using pristine NDC and Co-NDC. For OER, as shown in Figs. 4a and b, in general, the carbon and nitrogen sites on NDC plays a pivotal role in adsorbing H_2O molecules (step 1). Concurrently, photoexcited holes from nitrogen sites injected into H_2O molecules, forming *–OH (step 2). Subsequently, *–OH is converted into *–O (step 3), further converting into *–OOH (step 4). This conversion from *–OH to *–OOH is known as the RDS with a theoretical ΔG of 2.96 eV, higher than other steps [79]. Consequently, *–OOH is converted to O_2 molecules (step 5). Notably, when metal was incorporated on NDC, the oxidation steps still predominantly performed at nitrogen sites (step 6). While the photoexcited holes from the nitrogen sites were injected into the metal (step 7). The RDS is therefore promoted at the reactive metal sites, consequently leading to a substantial improvement in the OER rate (steps 7–10).

For ORR, the pristine NDC is insufficient for driving H_2O_2 production, as illustrated in Fig. 4c. In contrast, Fig. 4d illustrates the effective pathways for H_2O_2 production by Co-NDC. In the case of the pristine NDC, both carbon and nitrogen sites are capable of adsorbing O_2 molecules (step 11). But, under light illumination, the photoexcited electrons from carbon sites are unable to drive the conversion of the adsorbed O_2 molecule (step 12), probably due to a limitation imposed by the RDS (step 13). In the Co-NDC photocatalyst (Fig. 4d), as supported by the information provided in

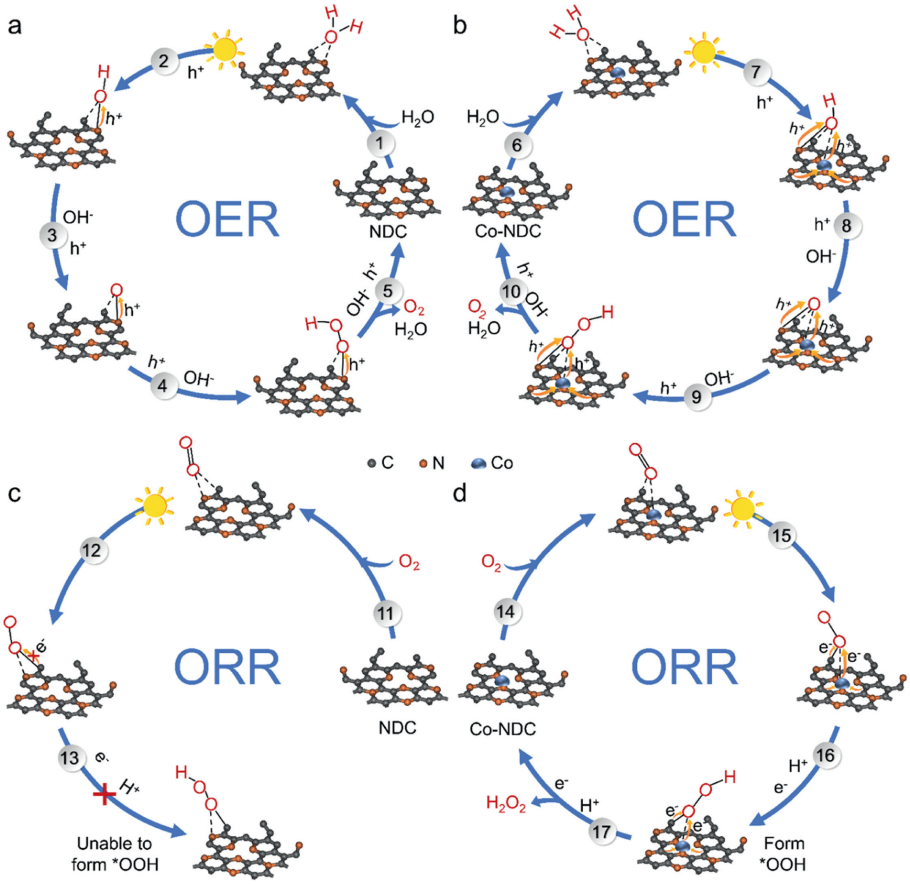

Fig. 4. The illustrations of the chemical pathways of OER on (a) NDC and (b) Co-NDC, and the chemical pathways of ORR on (c) NDC and (d) Co-NDC.

Fig. S9 (Supporting information), the presence of loaded Co species has a profound impact on the chemical environment of nitrogen sites. This interaction plays a crucial role in facilitating electron transfer processes involving C−O and N−O bonds. These electron transfers, in turn, activate O_2 and H_2O molecules adsorbed on the surface (step 14). Additionally, Co itself serves as active sites to active O_2, which was readily converted to CoOO* (steps 14 and 15). The CoOO* species was converted *OOH by the injection of a photoexcited electron under light illumination (step 16). Consequently, H_2O_2 was formed by hydrogenation of *OOH (step 17), and OER continues simultaneously (Fig. 4b).

In conclusion, NDC was synthesized by PE-CVD using NH_3 and CH_4 gases as precursors and various metals were loaded onto NDC to mimic the abundance of materials in the old Earth. The products were found to be effective photocatalysts that could drive both WOR and ORR under light illumination. The pristine NDC photocatalyst was active for OER in the presence of electron scavengers, and the OER rate was boosted by loading transition metals. More interestingly, the metal-loaded NDC has demonstrated the ability to catalyze ORR. The ORR was realized concurrently with OER to achieve an overall solar-to-chemical conversion. Of particular importance is our investigation into the underlying chemical pathways of OER and ORR on both pristine and metal-loaded NDC photocatalysts. Typically, carbon and nitrogen sites in NDC demonstrated activation in adsorbing and converting H_2O to O_2. The presence of metal on NDC further improved the OER performance by promoting the RDS, that is the conversion from *−OH to *−OOH. In the context of ORR for H_2O_2 production, carbon and nitrogen sites exhibited the capability to adsorb O_2 molecules but were insufficient for their conversion into H_2O_2. Importantly, the presence of metal on NDC enabled this conversion by facilitating the transformation of O_2 to *OOH, which represents the RDS in H_2O_2 production through ORR. The investigation of the photoactive material has provided valuable insights into the potential mechanisms relevant to the early evolution of Earth.

Declaration of competing interest

The authors declare that they have no known competing financial interests or personal relationships that could have appeared to influence the work reported in this paper.

CRediT authorship contribution statement

Yan Wang: Writing – original draft, Investigation, Formal analysis, Data curation, Conceptualization. **Jiaqi Zhang:** Validation, Investigation, Formal analysis. **Xiaofeng Wu:** Writing – review & editing, Visualization, Validation, Supervision. **Sibo Wang:** Writing – review & editing, Visualization, Validation, Supervision. **Masakazu Anpo:** Writing – review & editing, Visualization, Validation, Supervision. **Yuanxing Fang:** Writing – review & editing, Visualization, Validation, Supervision, Methodology, Formal analysis, Conceptualization.

Acknowledgments

This work was supported by the National Key Technologies R&D Program of China (Nos. 2022YFE0114800 and 2021YFA1502100), National Natural Science Foundation of China (Nos. 22075047, 22032002, U1905214, 21961142019) and the 111 Project (Nos. D16008).

Supplementary materials

Supplementary material associated with this article can be found, in the online version, at doi:10.1016/j.cclet.2024.110439.

References

[1] H. Reiche, A.J. Bard, J. Am. Chem. Soc. 101 (1979) 3127–3128.
[2] W.W. Dunn, Y. Aikawa, A.J. Bard, J. Am. Chem. Soc. 103 (1981) 6893–6897.
[3] N.C. Rockwell, S.S. Martin, J.C. Lagarias, Proc. Natl. Acad. Sci. U. S. A. 120 (2023) e2300770120.
[4] R.M. Soo, J. Hemp, D.H. Parks, et al., Science 355 (2017) 1436–1440.
[5] D.T. Johnston, F. Wolfe-Simon, A. Pearson, A.H. Knoll, Proc. Natl. Acad. Sci. U. S. A. 106 (2009) 16925–16929.
[6] P. Sánchez-Baracaldo, T. Cardona, New Phytol. 225 (2020) 1440–1446.
[7] L. Wang, Y. Kong, Y. Fang, et al., Adv. Funct. Mater. 32 (2022) 2208101.
[8] G. Jia, M. Sun, Y. Wang, et al., Adv. Funct. Mater. 32 (2022) 2206817.
[9] M. Liu, C. Wei, H. Zhuzhang, et al., Angew. Chem. Int. Ed. 61 (2022) e202113389.
[10] Z. Xie, W. Wang, X. Ke, et al., Appl. Catal. B: Environ. 325 (2023) 122312.
[11] Z. Luo, Y. Hou, J. Zhang, et al., Beilstein J. Org. Chem. 14 (2018) 2331–2339.
[12] Z. Hu, Z. Shen, J.C. Yu, Green Chem. 19 (2017) 588–613.
[13] Z.A. Lan, M. Wu, Z. Fang, et al., Angew. Chem. Int. Ed. 60 (2021) 16355–16359.
[14] S. Chai, X. Chen, X. Zhang, et al., Environ. Sci. 9 (2022) 2464–2469 Nano.
[15] N. Smirnoff, D. Arnaud, New Phytol. 221 (2019) 1197–1214.
[16] X. You, F. Zhang, Z. Liu, et al., Plant Physiol. 190 (2022) 1095–1099.
[17] Y. Wang, Y. Fang, Y. Wang, et al., Angew. Chem. Int. Ed. 62 (2023) e202307236.
[18] J. Korenaga, S. Marchi, Proc. Natl. Acad. Sci. U. S. A. 120 (2023) e2309181120.
[19] A.N. Halliday, Nature 427 (2004) 505–509.
[20] L.E. Rodriguez, Science 379 (2023) 539–540.
[21] C. Meyer, Science 227 (1985) 1421–1428.
[22] A. Bekker, M.E. Barley, M.L. Fiorentini, et al., Science 326 (2009) 1086–1089.
[23] J. Hao, W. Liu, J.L. Goff, et al., Sci. Adv. 8 (2022) eabn2226.
[24] E.K. Moore, J. Hao, A. Prabhu, et al., J. Geophys. Res.: Biogeo. 123 (2018) 743–759.
[25] J.D. Greenough, K. MacKenzie, Geosci. Can. 42 (2015) 351–367.
[26] S.S. Sun, Geochim. Cosmochim. Acta 46 (1982) 179–192.
[27] K. Righter, M. Schönbächler, K. Pando, et al., Earth Planet. Sci. Lett. 552 (2020) 116590.
[28] J.M. Trigo-Rodríguez, A. Rimola, S. Tanbakouei, et al., Space Sci. Rev. 215 (2019) 18.
[29] E.M.M.E. Van Kooten, D. Wielandt, M. Schiller, et al., Proc. Natl. Acad. Sci. U. S. A. 113 (2016) 2011–2016.
[30] M. Schiller, M. Bizzarro, J. Siebert, Sci. Adv. 6 (2020) eaay7604.
[31] S. Mostefaoui, C. Perron, E. Zinner, G. Sagon, Geochim. Cosmochim. Acta 64 (2000) 1945–1964.
[32] C. Lv, J. Liu, J. Geophys. Res.: Sol. Earth 127 (2022) e2021JB023718.
[33] R. Li, C. Zhang, K. You, et al., Chin. Chem. Lett. 34 (2023) 108801.
[34] Q. Lan, S. Jin, B. Yang, et al., Trans. Tianjin Univ. 28 (2022) 214–225.
[35] S. Liu, Q. Zhao, X. Han, et al., Trans. Tianjin Univ. 29 (2023) 293–303.
[36] Y. Xu, Y. Pan, W. Yahan, et al., Appl. Catal. B: Environ. 331 (2023) 122701.
[37] L. Wang, X. Cui, Y. Xu, et al., Chem. Commun. 58 (2022) 10469–10479.
[38] L. Yang, H. Chen, Y. Xu, et al., Chem. Eng. Sci. 251 (2022) 117435.
[39] L. Wang, P. Cai, Z. Liu, et al., J. Colloid Interface Sci. 607 (2022) 203–209.
[40] L. Xu, L. Li, Z. Hu, J.C. Yu, J. Catal. 418 (2023) 300–311.
[41] Y. Xu, Y. Cao, L. Tan, et al., J. Colloid Interface Sci. 633 (2023) 323–332.
[42] L. Li, Z. Hu, Y. Kang, et al., Nat. Commun. 14 (2023) 1890.
[43] G.h. Moon, M. Fujitsuka, S. Kim, et al., ACS Catal. 7 (2017) 2886–2895.
[44] C. Hu, H. Huang, F. Chen, et al., Adv. Funct. Mater. 30 (2020) 1908168.
[45] L. Li, L. Xu, Z. Hu, J.C. Yu, Adv. Funct. Mater. 31 (2021) 2106120.
[46] Z. Wang, S. Shen, Z. Lin, et al., Adv. Funct. Mater. 32 (2022) 2112832.
[47] Y. Fang, Y. Hou, X. Fu, X. Wang, Chem. Rev. 122 (2022) 4204–4256.
[48] C. He, F. Han, W. Zhang, Chin. Chem. Lett. 33 (2022) 404–409.
[49] W. Wu, Q. Zhang, X. Wang, et al., ACS Catal. 7 (2017) 7267–7273.
[50] F. Guo, W. Shi, C. Zhu, et al., Appl. Catal. B: Environ. 226 (2018) 412–420.
[51] Z. Pan, M. Zhao, H. Zhuzhang, et al., ACS Catal. 11 (2021) 13463–13471.
[52] Z. Chen, Y. Fang, L. Wang, et al., Appl. Catal. B: Environ. 296 (2021) 120369.
[53] S. Xue, W. Huang, W. Lin, et al., Chem. Catal. 2 (2022) 125–139.
[54] D. Zhou, X. Xue, Q. Luan, et al., Chin. Chem. Lett. 34 (2023) 107798.
[55] M. Zhong, D. Yang, C. Xie, et al., Small 12 (2016) 5564–5571.
[56] Y. Tang, W. Li, P. Feng, et al., Adv. Funct. Mater. 30 (2020) 1908754.
[57] S. He, J. Wang, X. Zhang, et al., Adv. Funct. Mater. 29 (2019) 1905228.
[58] S. Wang, Y. Hou, X. Wang, ACS Appl. Mater. Interfaces 7 (2015) 4327–4335.
[59] P. Wang, Y. Ren, R. Wang, et al., Nat. Commun. 11 (2020) 1576.
[60] S. Chen, S. Shen, G. Liu, et al., Angew. Chem. Int. Ed. 54 (2015) 3047–3051.
[61] J. Yang, D. Wang, H. Han, C. Li, Acc. Chem. Res. 46 (2013) 1900–1909.
[62] R. Shen, J. Xie, Q. Xiang, et al., Chin. J. Catal. 40 (2019) 240–288.
[63] Y. Li, W. Cheng, H. Su, et al., Nano Energy 77 (2020) 105121.
[64] X. Wang, J.C. Yu, P. Liu, et al., J. Photoch. Photobio. A 179 (2006) 339–347.
[65] J. Wu, Z. Liu, X. Lin, et al., Nat. Commun. 13 (2022) 6999.
[66] G. Gao, X. Wang, Q. Chen, et al., J. Mater. Chem. C 9 (2021) 1593–1603.
[67] Z. Wang, Y. Ding, J. Wang, Nanomaterials 9 (2019) 1397.
[68] N.G. Hădărugă, C.A. Chirilă, R.N. Szakal, et al., Foods 11 (2022) 3632.
[69] S. Zuo, Z.P. Wu, H. Zhang, X.W. Lou, Adv. Energy Mater. 12 (2022) 2103383.
[70] J. Wang, Y. Zhang, S. Jiang, et al., Angew. Chem. Int. Ed. 62 (2023) e202307808.
[71] Y. Lin, L. Yu, L. Tang, et al., ACS Catal. 12 (2022) 5345–5355.
[72] R. Takahashi, T. Noguchi, J. Phys. Chem. B 111 (2007) 13833–13844.
[73] J.C.S. Wu, Y.T. Cheng, J. Catal. 237 (2006) 393–404.
[74] G.M. Haselmann, B. Baumgartner, J. Wang, et al., ACS Catal. 10 (2020) 2964–2977.
[75] Y. Hao, X. Cao, C. Lei, et al., Mater. Today Catal. 2 (2023) 100012.
[76] J. Luo, X. Wei, Y. Qiao, et al., Adv. Mater. 35 (2023) 2210110.
[77] Y.X. Ye, J. Pan, F. Xie, et al., Porc. Natl. Acad. Sci. U. S. A. 118 (2021) e2103964118.
[78] W. Liu, P. Wang, J. Chen, et al., Adv. Funct. Mater. 32 (2022) 2205119.
[79] X. Chen, X. Wang, X. Zhang, et al., Int. J. Hydrogen Energy 46 (2021) 35198–35208.